Apical contractility in growing epithelium supports robust maintenance of smooth curvatures against cell-division-induced mechanical disturbance

Satoru Okuda[a], Yasuhiro Inoue[a], Mototsugu Eiraku[b], Yoshiki Sasai[c], Taiji Adachi[a,*]

[a]*Department of Biomechanics, Institute for Frontier Medical Sciences, Kyoto University, Kyoto 606-8507, Japan*
[b]*Four-Dimensional Tissue Analysis Unit, Center for Developmental Biology, RIKEN, Kobe 650-0047, Japan*
[c]*Organogenesis and Neurogenesis Group, Center for Developmental Biology, RIKEN, Kobe 650-0047, Japan*

Abstract

In general, a rapidly growing epithelial sheet during tissue morphogenesis shows a smooth and continuous curvature on both inner cavity (apical) and basement membrane (basal) sides. For instance, epithelia of the neural tube and optic vesicle in the early embryo maintain continuous curvatures in their local domains, even during their rapid growth. However, given that cell divisions, which substantially perturb the local force balance, frequently and successively occur in an uncoordinated manner, it is not self-evident to explain how the tissue keeps a continuous curvature at large. In the majority of developing embryonic epithelia with smooth surfaces, their curvatures are apically concave, because of the presence of strong tangential contractile force on the apical side. In this numerical study, we demonstrate that tangential contractile forces on the apical surface plays a critical role in the maintenance of smooth curvatures in the epithelium and reduces irregular undulations caused by uncoordinated generation of local pushing force. Using a reversible network reconnection (RNR) model, which we previously developed to make numerical analyses highly reproducible even under rapid tissue-growth conditions, we performed simulations for morphodynamics to examine the effect of apical contractile forces on the continuity of curvatures. Interestingly, the presence of apical contractile forces suppressed irregular undulations not only on the apical side, but also on the basal surface. These results indicate that cellular contractile forces on the apical surface control not only the shape at a single cell level, but also at a tissue level as a result of emergent mechanical coordination.

Keywords: Tissue morphogenesis, Multicellular dynamics, Three-dimensional vertex model, Reversible network reconnection model, Developmental biomechanics

1. Introduction

During development of multicellular organisms, tissues deform into complex organ shapes in a three-dimensional (3D) manner. The complex shaping is achieved by the balance of mechanical forces, which are generated by cell activities such as cell contraction and cell proliferation. However, how these events at the cell level eventually lead to the structure formation at the tissue level remains elusive in most cases of organ development.

An epithelial sheet is a basic structure that is frequently seen in many aspects of organogenesis, and commonly has smooth surface curvatures on both apical and basal sides. Such smooth curvatures can be observed in, for instance, the neural tube and optic vesicle in the early embryo, which give rise to the brain and retina, respectively (Nishimura et al., 2012; Weaver et al., 2001; Zolessi et al., 2001; Eiraku et al., 2011, 2012). However, it is not simple to explain how these smooth surface curvatures are maintained in these rapidly growing tissues, because the force balance among cells is locally changed by cell divisions, which successively occur with spatiotemporally random timing. Our previous numerical investigation suggested that cell proliferation tends to induce irregular undulation of sheet-shaped tissue (Okuda et al., 2012a,b). To maintain the smooth epithelial curvatures during successive rounds of cell proliferation, the configurations of proliferating cells need to be constrained in the plane of the epithelial sheet.

The smooth epithelia in such embryonic structures as the neural tube and optic vesicles are apically concave. One common feature found in the apical end of these epithelia is that actomyosin is homogeneously and densely accumulated as a circumferential belt in each cell (Nishimura et al., 2012; Weaver et al., 2001; Zolessi et al., 2001; Eiraku et al., 2011, 2012). This circumferential actomyosin belt is known to generate tangential contractile force on the apical surface at the cell level, and contributes to deformation in cell shape and rearrangement in geometrical patterns (Lecuit and Lenne, 2007; Lecuit et al., 2010). This implies that the contractile force may affect 3D tissue shapes and configurations, e.g., the curvatures of epithelial sheets. Consistent with this idea, previous Drosophila studies have shown that local control of actomyosin causes a change in tissue curvature via the apical constriction during mesoderm invagination (Martin et al., 2010). A similar observations were reported in the vertebrate studies of eye cup formation (Weaver

*Corresponding author at: Department of Biomechanics, Institute for Frontier Medical Sciences, Kyoto University, 53 Kawahara-cho, Shogoin, Sakyo-ku, Kyoto 606-8507, Japan. Tel./fax: +81 75 751 4853.
Email address: adachi@frontier.kyoto-u.ac.jp (Taiji Adachi)

et al., 2001; Zolessi et al., 2001; Eiraku et al., 2011, 2012) and neural tube formation (Nishimura et al., 2012).

On the basis of these reports, we became interested in the idea that tangential contractile force on the apical surface maintains smooth curvatures of epithelium by preventing it from undulating irregularly during tissue growth. In rapidly growing epithelia, substantial mechanical disturbances are given internally by irregular pushing forces locally induced by cell divisions. The question is whether the contractile force along the apical actin belt at the cell level is sufficient to overcome these uncoordinated perturbations for smoothening the epithelial structure at the tissue level.

To analyze multicellular dynamics during the 3D morphogenesis, 3D vertex models have been proposed (Honda et al., 2004). A conventional 3D vertex model has been successfully used for simulating tissue morphogenesis, such as the polarization process in the preimplantation mouse embryo (Honda et al., 2008a) and tissue extensions driven by cellular intercalations (Honda et al., 2008b). However, the conventional 3D vertex model has a limitation for simulating complex deformations because of problems in the reconnection of vertices. To resolve them, we have developed a reversible network reconnection (RNR) model (Okuda et al., 2012a), and successfully applied it to the simulation study of complex deformations induced by successive rounds of cell proliferation (Okuda et al., 2012b). Thus, the RNR model provides a useful tool for analyzing morphogenesis of epithelium with high cell proliferation.

In this study, we use the RNR model to evaluate the contribution of the contractile force, generated by circumferential actomyosin belt, to the maintenance of smooth curvatures of epithelium. By simulating the morphodynamics of epithelial sheets with cell proliferation with the RNR model, we demonstrate that the presence of apical contractile force is critical for preventing the epithelium from undulating irregularly during tissue growth.

2. Reversible network reconnection Simulation

2.1. Modeling multicellular dynamics

Multicellular dynamics during tissue morphogenesis was mathematically expressed using the RNR model (Okuda et al., 2012a). In the RNR model, the shape of a cell is represented by a polyhedron. This polyhedron includes vertices and edges that are shared by neighboring polyhedrons. These vertices and edges comprise a network that represents the entire shape of the aggregate. In this network, each vertex is connected to four edges. Moreover, neighboring polyhedrons are compartmentalized by these polygonal faces. The shape of a polygonal face that has four or more edges is defined as radially arranged triangles composed of each edge and the center point of the polygonal face (Okuda et al., 2012a).

To express the multicellular dynamics within aggregates, an equation for the motion of the ith vertex was introduced as follows:

$$\eta \frac{d\boldsymbol{r}_i}{dt} = -\frac{\partial U}{\partial \boldsymbol{r}_i}. \tag{1}$$

The left-hand side of Eq. (1) is a frictional force that is exerted on the ith vertex, where η is a friction coefficient and $\boldsymbol{r}_i$ is the position vector of the ith vertex. The right-hand side of Eq. (1) is a conservative force, where U represents the potential energy of cells. In addition, cell rearrangements within an aggregate are expressed by reconnecting local network patterns (Okuda et al., 2012a). In this network reconnection, because cells are strongly connected by tight junctions located near their apical surfaces (Tsukita et al., 2001), it is assumed that each cell cannot lose its apical surface.

Cell proliferation was expressed using a cell proliferation model (Okuda et al., 2012b), in which cell proliferation was characterized both by cell division (increase in cell number) and cell growth (increase in cell volume) (Fig. 1a). In addition, cell division was represented by dividing a single polyhedron at a plane. Direction of the dividing plane is locally regulated to the longest axis of cell shape in the plane of epithelial sheet normal to the apicobasal direction (Fig. 1b). Details of the cell division manner are described in Supplementary information S1, which are similar to those of the local regulation used in our previous study (Okuda et al., 2012b).

Cell mechanical properties and reference states were simply expressed using the potential energy, U, (Fig. 1c) as follows:

$$U = \sum_{i}^{\text{cell}} \left(u_i^{\text{cv}} + u_i^{\text{cs}} + u_i^{\text{ch}} + u_i^{\text{ac}} \right), \tag{2}$$

where $\sum_i^{\text{cell}}$ indicates the summation for all cells. Here u_i^{cv} is the cell volume elastic energy , u_i^{cs} is the cell surface elastic energy , u_i^{ch} is the cell height elastic energy , and u_i^{ac} is the apical contractile energy. Functions of these potential energies are described in Supplementary information S2.

2.2. Simulation conditions

To investigate the effects of apical contractility on the continuity of curvatures in growing epithelia, we simulated the morphodynamics of tissues consisting of proliferating cells. To solve Eq. (1), parameter values were normalized by unit length (l), unit time (τ), and unit energy (k_BT). Here l and τ were set at $l = (v_0)^{\frac{1}{3}}$ and $\tau = \tau_{\text{ave}}^{\text{cell cycle}}$.

As an initial condition, we chose a spherical shell configuration, in which proliferating cells were located in a monolayer sheet. This is because a spherical shell with a homogeneous curvature is appropriate for analyzing mechanical effects of cell behaviors on a tissue curvature. In addition, such spherical shell configurations can be observed in cavitation processes of stem cell aggregates, and hemispherical shell configurations can be observed in processes of regeneration of an optic-cup (Eiraku et al., 2011, 2012). The number of proliferating cells under this initial condition was set to $n_0^{\text{c}} = 258$. An apical surface was inside the spherical shell. Each cell time, t_i^{c}, for the initial condition was randomly determined.

The standard deviation of cell division times, $\tau_{\text{sd}}^{\text{cell cycle}}$, was set at $0.1\tau_{\text{ave}}^{\text{cell cycle}}$. Numerical integration of Eq. (1) over time used the Euler method with a time step of Δt. Local network patterns were reconnected when each edge included in a local

pattern became shorter than a threshold value, $\Delta l_{\rm th}$. Trials for applying the reconnection rule were conducted for each edge, and each trigonal face at each of the $\Delta t_r/\Delta t$ steps ($\Delta t_r \geq \Delta t$). All model parameters are shown in Table 1.

3. Results

3.1. Apical contractility supports to maintain smooth curvatures of epithelial sheet

To investigate the effects of apical contractility on the maintenance of the smooth epithelial curvatures, we simulated the morphodynamics of growing tissues with and without apical contractility. First, to clarify that smooth curvatures can be maintained in a case with apical contractility, we simulated the morphodynamics of a tissue with apical contractility, $k^{\rm ac} = 1.0$, during the whole time period from $t = 0$. Second, to compare this result to that without apical contractility, we inhibited the apical contractility computationally to be $k^{\rm ac} = 0$ from the tissue that resulted from simulations with apical contractility at $t = 1$.

Figure 2 shows several snapshots that illustrate the temporal evolution of growing tissues for the cases with and without apical contractility. These morphogenetic processes are also shown in Supplementary Movies 1 and 2. Visual inspection of Fig. 2a-h indicates that for the case with apical contractility, the tissue grows while maintaining the smooth curvatures of both the apical and basal surfaces. In contrast, for the case without apical contractility (Fig. 2i), the tissue deforms out of the plane and curvatures of both its apical and basal surfaces become rough (Fig. 2j-m). Smooth surfaces begin to disappear soon after $t = 1$, when apical contractility began to be inhibited. These results indicate that apical contractility supports to maintain smooth curvatures during growth.

Figure 3 shows the standard deviations (SDs) of mean curvatures, $C_{\rm H}$, on epithelial surfaces as a function of time. During the early time period, $t < 0.5$, SDs on apical surfaces with apical contractility decreased with time and approached a constant value. This appears to occur because initial strains inside the tissue are relaxed by the mechanical disturbances of cell proliferation. During the late time period, $t > 0.5$, in cases with apical contractility, SDs of $C_{\rm H}$ slightly increased with time. These increases imply that the epithelial surfaces could become undulated in the longer time region. In contrast, in cases without apical contractility, SDs significantly increased from $t = 1$, and became approximately an order of magnitude higher than those with apical contractility. This result suggested that apical contractility has the effect of maintaining smooth curvatures.

3.2. Apical contractility affects the uniformity of cell shapes

To understand the effects of apical contractility on cell shape and configuration, we analyzed the time variations of cell shapes and configurations as shown in Fig. 4. Visual inspection of Fig. 4b and c indicates that with apical contractility, cell shapes were uniform and cell configuration was constrained in the plane of an epithelial sheet. In contrast, for the case without apical contractility, as shown in Fig. 4e, cells deformed to be cone-like shapes of which the apex sides were alternately directed toward both the apical and basal sides. These cell shapes and configurations correspond to geometrical cell patterns on apical surfaces, as shown in Fig. 4f and g, in which cell sizes with apical contractility are homogeneous, whereas those without apical contractility are inhomogeneous. These results suggested that apical contractility affected the uniformity of cell shapes, which was related to the continuity of tissue curvatures.

3.3. Apical contractility suppresses cell-division-induced pushing forces

To understand the effects of apical contractility on cell deformations, we analyzed the stress distributions for each cell (Fig. 5a, c) and each apical or basal polygonal face (Fig. 5b, d). Stresses are drawn with apical contractility (Fig. 5a, b) and without apical contractility (Fig. 5c, d). Figure 5a and Figure 5c show the average stresses within each cell in the tangent plane of epithelial sheets, $(\sigma^{\rm c}_{x'x'(i)} + \sigma^{\rm c}_{y'y'(i)})/2$, which were estimated by assuming a homogeneous stress state within each cell. Here $\sigma^{\rm c}_{\alpha'\beta'(i)}$ indicates the α' β' component of a stress tensor locally defined for the ith cell coordinate defined in Fig. 1b. A component of the stress inside the ith cell, $\sigma^{\rm c}_{\alpha'\beta'(i)}$, is estimated using the following method (Hardy, 1982).

$$\sigma^{\rm c}_{\alpha'\beta'(i)} = \frac{1}{v^{\rm c}_i} \sum_{j(i)}^{\rm vertex} \left(\boldsymbol{r}_j\right)_{\alpha'} \left(\boldsymbol{f}_j\right)_{\beta'}, \tag{3}$$

where $\sum_{j(i)}^{\rm vertex}$ is the summation over all vertices composing the ith cell. Bracket $(...)_{\alpha'}$ indicates the α' component of the vector enclosed in parentheses. Force $\boldsymbol{f}_j$ is calculated as $-\partial\left(u^{\rm cv}_i + u^{\rm cs}_i + u^{\rm ch}_i + u^{\rm ac}_i\right)/\partial \boldsymbol{r}_j$. As shown in Fig. 5a and c, tangential stresses within cells were negative. This indicated that cells were pushing the surrounding cells in the tangent plane with and without apical contractility. Thus, the morphodynamics of growing tissues basically progressed under compressive conditions at the single cell level.

Figure 5b and Figure 5d show the average in-plane stresses within each apical or basal polygonal face, $(\sigma^{\rm s}_{x'x'(k(i))} + \sigma^{\rm s}_{y'y'(k(i))})/2$, which were estimated by assuming a homogeneous stress state within each face. A component of the stress inside the kth polygonal face in the ith cell, $\sigma^{\rm s}_{\alpha'\beta'(k(i))}$, is estimated using the following method (Hardy, 1982).

$$\sigma^{\rm s}_{\alpha'\beta'(k(i))} = \frac{1}{s^{\rm c}_i} \sum_{j'(k(i))}^{\rm vertex} \left(\boldsymbol{r}_{j'}\right)_{\alpha'} \left(\boldsymbol{f}^{\parallel}_{j'}\right)_{\beta'}, \tag{4}$$

where $\sum_{j'(k(i))}^{\rm vertex}$ is the summation over all vertices composing the kth polygonal surface in the ith cell. Force $\boldsymbol{f}^{\parallel}_{j'}$ is the vector of $\boldsymbol{f}_{j'}$ projected into the plane of the kth polygonal face. Here the plane of the kth polygonal face was approximately defined by the plane normal to a vector, $\boldsymbol{n}^{\rm pf}_k$:

$$\boldsymbol{n}^{\rm pf}_k = \frac{\sum^{\rm tri}_{l(k)} s^{\rm tri}_{l(k)} \boldsymbol{n}^{\rm tri}_{l(k)}}{\sum^{\rm tri}_{l(k)} s^{\rm tri}_{l(k)}}. \tag{5}$$

where $\sum_{l(k)}^{\mathrm{tri}}$ indicates the summation of triangles comprising the kth polygonal face. The variable $s_{l(k)}^{\mathrm{tri}}$ and vector $\boldsymbol{n}_{l(k)}^{\mathrm{tri}}$ are the surface area and the normal vector of the lth triangle in the kth polygonal face, respectively. As shown in Fig. 5b, for the case with apical contractility, in-plane stresses at the apical surface were positive (tension), while those at the basal surface were negative (compression). This indicated that cells were contracting at their apical surfaces and expanding at their basal surfaces at the subcellular level. These results suggest that even when cells are under compressive conditions at the single cell level, cells can be partially under tensile conditions at the subcellular level. On the other hand, as shown in Fig. 5d, for the case without apical contractility, both apical and basal surfaces are under compression conditions.

3.4. Height elasticity works to maintain cell heights, but not smooth curvatures

To highlight the effect of apical contractility on the maintenance of smooth curvatures, we investigated whether the elastic energy of cell height U^{ch} affects the maintenance of smooth curvatures. To determine this, we simulated the morphodynamics without the height elastic energy, $k^{\mathrm{ch}} = 0$, as shown in Fig. 6. Even in cases without the height elastic energy, the maintenance of smooth curvatures depends on apical contractility (Fig. 6a and b), similar to that in cases with the height elastic energy (Fig. 2h and m). Moreover, the gradient in cell heights in the case with height elastic energy is weaker than that without height elastic energy (Fig. 6c and d). Thus, the height elastic energy works to maintain cell heights, but not smooth curvatures. These results underscore the effect of apical contractility on the maintenance of smooth curvatures.

3.5. Dependence of curvatures on the strength of surface elasticity

To determine the effect of the surface elastic energy on curvatures, we simulated the morphodynamics in cases with various values of the surface elasticity, $0.0256 \leq k^{\mathrm{cs}} \leq 256$, as shown in Fig. 7. Interestingly, in cases with low values of the surface elasticity, $k^{\mathrm{cs}} \leq 0.256$, the epithelial sheet maintains a smooth curvature on its apical surface but not on its basal surface (Fig. 7a and b). In cases with high values of the surface elasticity, $k^{\mathrm{cs}} \geq 2.56$, the epithelial sheet maintains smooth curvatures on both its apical and basal surfaces (Fig. 7c and d). These results suggest that the cell surface elasticity can smoothen basal surfaces on the basis of smooth apical surfaces.

3.6. Dependence of curvatures on the strength of apical contractility

To analyze the dependence of curvatures on the strength of apical contractility, we simulated the morphodynamics of epithelial sheets with various strengths of apical contractility, k^{ac}, as shown in Fig. 8. In each case, epithelial sheets grew due to cell proliferation for the time period $0 \leq t \leq 2$ with a specific value of k^{ac}. Figure 8a shows SDs of mean curvatures, C_{H}, of epithelial sheets. In cases with weak contractility, $k^{\mathrm{ac}} \leq 10^{-2}$, SDs of C_{H} were constantly high (Fig. 8a), and both apical and basal surfaces are undulated (Fig. 8c and d). In cases with moderate values of apical contractility, $10^{-2} \leq k^{\mathrm{ac}} \leq 10^{0}$ (Fig. 8a), SDs of C_{H} were drastically decreased, and the undulations of apical and basal surfaces became suppressed with increasing k^{ac} (Fig. 8d and e). In cases with strong contractility, $k^{\mathrm{ac}} \geq 10^{0}$, SDs of C_{H} were constantly low (Fig. 8a), and both apical and basal surfaces were smooth (Fig. 8e and f). These results suggested that epithelial undulations can depend on the strength of apical contractility.

In addition, to compare the simulation results with experimental ones, we measured the strains of cell apical widths as a function of k^{ac} (Fig. 8b). To measure the strains, relaxation simulations were performed for the epithelial sheets while omitting cell proliferation and apical contractility, $k^{\mathrm{ac}} = 0$, for the time period $2.0 < t < 2.5$. The strains were estimated from the square roots of the average surface areas of the apical polygons at $t = 2.0$ and 2.5. The strains of the cell apical widths increased exponentially with apical contractility. Remarkably, at least in the range of k^{ac} values employed in this study, the resulting strains showed values less than 0.68 (Plageman et al., 2011), which was measured by experiments with biochemical inhibitions, resulting in reduced apical contractility during invagination processes. Therefore, from a geometrical viewpoint, the strength of the apical contractility employed in this study could be physiologically natural or weaker than that in the experiments. Thus, these results support the demonstrated effect of apical contractility on the maintenance of smooth curvatures.

4. Discussion

To determine the mechanical effects of apical contractility on the maintenance of smooth curvatures of growing epithelia, we performed RNR simulations for the morphodynamics of a spherical shell-shaped epithelial sheet with apically concave structure. These results showed that the presence of apical contractility supported the maintenance of smooth curvatures of an epithelial sheet not only on apical, but also on basal surfaces (Fig. 2). These results indicate that cellular contractile forces on the apical surface control not only the shape at the single cell level, but also at the tissue level as a result of emergent mechanical coordination. Because the smooth curvatures of the epithelial sheet are qualitatively independent of the height elastic energy, as shown in Fig. 6, apical contractility is relatively important in maintaining smooth curvatures.

For the case without apical contractility, the epithelial sheet deformed out of its tangent plane and its curvatures became rough (Fig. 2f and g). This was because at the single cell level and at the subcellular level, the force balance among cells were perturbed by irregular pushing forces generated by cell divisions (Fig. 5c, d). Cell proliferation increased cell volumes, which exerted pushing force on surrounding cells throughout the entire area of cell–cell boundaries. Because cell divisions occur with spatiotemporally random timing, the pushing forces became inhomogeneous in the tissue level. Because cells could deform to be cone-like shapes in which their apex sides can be directed toward both the apical and basal sides, cells could be extruded from the tangent plane of the epithelial sheet under

the compressive condition for the entire area of the cell–cell boundaries (Fig. 4d, e).Thus, cell divisions with spatiotemporally random timing induced the mechanical disturbance in the force balance among cells, which undulated epithelia irregularly.

For the case with apical contractility, smooth curvatures were maintained on both apical and basal surfaces in the tissue level (Fig. 2c and d). This was because apical contractility at each cell generated the tensile forces on the apical surface of the epithelial sheet (Fig. 5b). This tensile force smoothed the apical surface of the epithelial sheet in the tissue level. In addition, this tensile force made cells to be cone-like shapes, in which their apex sides were uniformly directed toward the apical side of the tissue (Fig. 4b, c). Because these uniformly directed cells were aligned on the smooth apical surface, the smooth curvatures were maintained on apical surface. Furthermore, because these regularly aligned cells have similar heights to each other, the smooth curvatures were also maintained on basal surface. Thus, apical contractility coordinates cell locations and deformations, which leads to suppressing the undulation of epithelial sheet induced by cell divisions.

Apical contractility deforms cells into cone-like shapes oriented in the same apicobasal direction (Fig. 4b and c). Such cell shapes characteristics and orientation have been reported in previous experimental studies with biochemical inhibitions, resulting in reduced apical contractility during invagination processes (Plageman et al., 2011). Moreover, in previous experimental studies, such inhibitions led to the expansion of apical areas of cone-like cell shapes (Kinoshita et al., 2008; Nishimura et al., 2008; Plageman et al., 2011). Therefore, the results of the present simulations show cell deformations that are physiologically similar to those observed in previous experiments.

In addition to individual cell shapes, the geometrical cell patterns on the apical surfaces of epithelium are also characteristic. As shown in Fig. 4f and g, the sizes of cells on apical surfaces with apical contractility are homogeneous, whereas the sizes of cells on apical surfaces without apical contractility are inhomogeneous. The difference in cell sizes in the present study is similar to that reported by a previous study based on a 2D vertex model (Farhadifar et al., 2007), in which numerical simulations demonstrated 2D geometrical cell patterns. These qualitative consistencies between the present and past studies physiologically support the demonstrated effect of apical contractility on the maintenance of smooth curvatures.

To demonstrate the effect of apical contractility more convincingly, the simulation results should be validated based not only on cell geometries but also on cell mechanical properties. For instance, sensitivity analyses based on varying cell mechanical properties will be useful to make comprehensive predictions of their effects on morphogenesis. Moreover, these predictions could be buttressed by experimental measurements using mechanical perturbations (Farhadifar et al., 2007).

In this study, to focus only on the mechanical effects of apical contractility, certain cell mechanical properties and activities were simply assumed. That is, the mechanical effects due to other properties and activities were ignored, except for apical contractility and cell proliferation. For example, the bending rigidity of a basement membrane can affect curvatures of epithelia. In addition to proliferation, cellular apoptosis and the epithelial-mesenchymal transition can change the local tissue volume. These cell properties and activities might contribute to regulation of tissue curvatures. However, these factors may not require modification of our findings regarding the effects of apical contractility on the maintenance of smooth curvatures. Rather, these additional factors might enforce the maintenance of smooth curvatures. For example, curvatures of epithelia could be regulated by apoptosis, which can be regulated by pressure on cells (Shraiman, 2005). Also, the bending rigidity of basement membrane might contribute to the maintenance of smooth curvatures. Thus, it was worth focusing on the mechanical effects of apical contractility as a possible candidate involved in this mechanism.

In conclusion, we investigated the mechanical effects of apical contractility on the maintenance of the smooth curvatures of epithelium under the mechanical disturbance generated by cell divisions. RNR simulation results showed that the presence of apical contractility suppressed the disturbance in the force balance among cells so as to avoid epithelial sheets from undulating irregularly during tissue growth. This was because apical contractility coordinates individual cell locations and deformations in the tissue level. Thus, apical contractility has a critical role to support robust maintenance of smooth curvatures against cell-division induced mechanical disturbance.

Conflicts of interest

There is no financial and personal relationship with other people or organizations that could inappropriately influence this work.

Acknowledgments

This work was partially supported by the Funding Program for Next Generation World-Leading Researchers (LR017) from the Ministry of Education, Culture, Sports, Science and Technology (MEXT) in Japan. Satoru Okuda was supported by the Japan Society for the Promotion of Science (JSPS) as a JSPS fellow. Yasuhiro Inoue was supported by "Morphologic" (23127506) Grant-in-Aid for Scientific Research on Innovative Areas, MEXT, Japan.

References

Eiraku, M., Adachi, T., et. al., 2012. Relaxation-expansion model for self-driven retinal morphogenesis. Bioessays 34 (1), 17-25.

Eiraku, M., Takata, N., et. al., 2011. Self-organizing optic-cup morphogenesis in three-dimensional culture. Nature 472 (7341), 51-56.

Farhadifar, R., Röper, JC., et. al., 2007. The influence of cell mechanics, cell–cell interactions, and proliferation on epithelial packing. Curr Biol 17 (24), 2095-2104.

Gibson, WT., Veldhuis, JH., et. al., 2011. Control of the mitotic cleavage plane by local epithelial topology. Cell 144 (3), 427-438.

Hardy, RJ., 1982. Formulas for determining local properties in molecular–dynamics simulations: Shock waves. J Chem Phys 76(1), 622-628.

Honda, H., Motosugi, N., et. al., 2008. Computer simulation of emerging asymmetry in the mouse blastocyst. Development 135 (8), 1407-1414.

Honda, H., Nagai, T., et. al., 2008. Two different mechanisms of planar cell intercalation leading to tissue elongation. Dev Dyn 237 (7), 1826-1836.

Honda, H., Tanemura, M., et. al., 2004. A three-dimensional vertex dynamics cell model of space-filling polyhedra simulating cell behavior in a cell aggregate. J Theor Biol 226 (4), 439-453.

Kinoshita, N., Sasai, N., et al., 2008. Apical accumulation of Rho in the neural plate is important for neural plate cell shape change and neural tube formation. Mol Biol Cell 19(5), 2289-2299.

Lecuit, T., Lenne, PF., 2007. Cell surface mechanics and the control of cell shape, tissue patterns and morphogenesis. Nat Rev Mol Cell Biol 8 (8), 633-644.

Lecuit, T., Rauzi, M., et. al., 2008. Nature and anisotropy of cortical forces orienting Drosophila tissue morphogenesis. Nat Cell Biol 10 (12), 1401-1410.

Lecuit, T., Rauzi, M., et. al., 2010. Planar polarized actomyosin contractile flows control epithelial junction remodelling. Nature 468 (7327), 1110-1114.

Martin, AC., Gelbart, M., et. al., 2010. Integration of contractile forces during tissue invagination. J Cell Biol 188 (5), 735-749.

Nishimura, T., Takeichi, M., 2008. Shroom3-mediated recruitment of Rho kinases to the apical cell junctions regulates epithelial and neuroepithelial planar remodeling. Development 135(8), 1493-1502.

Nishimura, T., Honda, H., et. al., 2012. Planar cell polarity links axes of spatial dynamics in neural-tube closure. Cell 149 (5), 1084-1097.

Noguchi, H., Gompper, G., 2005. Dynamics of fluid vesicles in shear flow: Effect of membrane viscosity and thermal fluctuations. Phys Rev E 72 (1), 11901-11914.

Okuda, S., Inoue, Y., et. al., 2012a. Reversible network reconnection model for simulating large deformation in dynamic tissue morphogenesis. Biomech Model Mechanobiol (in press).

Okuda, S., Inoue, Y., et. al., 2012b. Modeling cell proliferation for simulating three-dimensional tissue morphogenesis based on a reversible network reconnection framework. Biomech Model Mechanobiol (in press).

Plageman, TF. Jr., Chauhan, BK., et. al., 2011. A Trio-RhoA-Shroom3 pathway is required for apical constriction and epithelial invagination. Development 138(23), 5177-5188.

Shraiman, BI., 2005. Mechanical feedback as a possible regulator of tissue growth. Proc Natl Acad Sci U S A. 102 (9), 3318-3323.

Tsukita S, Furuse M, Itoh M. 2001. Multifunctional strands in tight junctions. Nat Rev Mol Cell Biol. 2 (4), 285-293.

Ujihara, Y., Nakamura, M., et. al., 2005. Proposed spring network cell model based on a minimum energy concept. Ann Biomed Eng 38 (4), 1530-1538.

Weaver, M., Hogan, B., 2001. Powerful ideas driven by simple tools: lessons from experimental embryology. Nature Cell Biology 3 (7), E165 - E167.

Zolessi, FR., Arruti, C., 2001. Apical accumulation of MARCKS in neural plate cells during neurulation in the chick embryo. BMC Dev Biol 1, 7.

Table and figure captions

Table 1: Model parameters

Fig. 1: Epithelial cell division behaviors and mechanical properties. (a) Cell proliferation processes. A cell divides into two daughter cells, which grow by increasing their reference volume. (b) Cell coordinates. Orthogonal coordinates, x'-y'-z', were defined for each cell by setting the z'-axis to include two points: the center of inertia of the ith cell, $\boldsymbol{g}_i^{\mathrm{c}}$, and the polygonal center of its apical surface, $\boldsymbol{r}_i^{\mathrm{pc(as)}}$. (c) Cell mechanical properties. Cell volume, v_i^{c}, is maintained to be approximately constant. Cell surface area, s_i^{c}, is constrained for the whole surfaces of each cell. Cell height, l_i^{ch}, is individually constrained by a spring inserted between the center points of the apical and basal surfaces. In addition, the circumferential length of the apical surface, l_i^{ac}, is contracted by apical contractility. The cell mechanical properties are expressed by potential energies as shown in the right box. Here u_i^{cv} is the cell volume elastic energy, u_i^{cs} is the cell surface elastic energy, u_i^{ch} is the cell height elastic energy, and u_i^{ac} is the apical contractile energy. Constants k_i^{cv}, k_i^{cs}, k_i^{ch}, and k_i^{ac} indicate elastic constants in the respective potential energies. Subscript eq indicates equilibrium values of individual parameters. Details of these functions are described in Supplementary information S2.

Fig. 2: Morphodynamics of proliferating tissues *in silico*. (a-d) Snapshots of the entire shapes of tissues proliferating in the presence of apical contractility: $k_{\mathrm{ac}} = 1.0$. (e-h) Cross-sections of tissues cut at the white line in (a-d). (i) Changes in cell mechanical properties after excluding apical contractility: $k_{\mathrm{ac}} = 0.0$ at $t = 1.0$ without apical contractility. (j, k) Snapshots of entire shapes of tissues proliferating in the absence of apical contractility.
(l, m) Cross-sections of tissues cut at the white line in (j, k). Times for these snapshots are $t = 0$, 1.0, 1.5, and 2.0 in order from left. Tissues consisting of n^{c} cells. Colors on the apical or basal surface in (a-h, j-m) indicate mean curvatures C_{H} measured from the surfaces of several cells surrounding a single cell.

Fig. 3: Standard deviations (SDs) of the mean curvatures, C_{H}, of epithelial surfaces, as a function of time, t. SDs of apical (pink) and basal (blue) surfaces were estimated in cases with apical contractility (solid line) and without apical contractility (dotted line).

Fig. 4: Snapshots of several cell shapes and configurations. Colored polyhedrons represent individual cell shapes in 3D space. Cell colors indicate the differences between apical and basal circumferential lengths, $\Delta l^{\mathrm{b\text{-}a}}$. In cases where the apex side of a cone-like cell is directed toward the apical side, $\Delta l^{\mathrm{b\text{-}a}}$ becomes positive, and vice versa. Black lines indicate surrounding cell shapes at cross-sections of tissues. (a, b, and c) Several cell shapes and configurations for the case with apical contractility. (d, e) Several cell shapes and configurations for the case without apical contractility. Times for these snapshots are $t = 1.0$ (a), 1.5 (b, d), and 2.0 (c, e) in order from left. (f, g) Geometrical cell patterns on the apical side at $t = 1.5$ in cases with apical contractility (f) and without apical contractility (g).

Fig. 5: Distributions of intracellular stresses in tissues. (a-b) Stress for the case with apical contractility at $t = 2.0$. (c-d) Stress for the case without apical contractility at $t = 2.0$. (a, c) The average normal stress within each cell in the epithelial plane, $(\sigma_{x'x'} + \sigma_{y'y'})/2$, was estimated by assuming a homogeneous stress state within each cell. (b, d) In-plane stress within each apical or basal polygonal face, which was estimated by assuming a homogeneous stress state within each face.

Fig. 6: Effects of the height elasticity on curvatures. (a, b) Snapshots of tissues without height elastic energy, $k^{\mathrm{ch}} = 0.0$, at $t = 2.0$. The tissues are shown for cases with apical contractility, $k^{\mathrm{ac}} = 1.0$ (a), and without apical contractility, $k^{\mathrm{ac}} = 0.0$ (b). Colors on the apical and basal surfaces indicate mean curvatures, C_{H}. (c) The average of normalized cell heights, $< l_i^{\mathrm{ch}}/l_{\mathrm{eq}}^{\mathrm{ch}} >$, as a function of time, t, in the case with apical contractility, $k^{\mathrm{ac}} = 1.0$. (d) Comparison of tissue cross-sections at $t = 2.0$ in cases with the height elastic energy, $k^{\mathrm{ch}} = 10.0$ (left), and without the height elastic energy, $k^{\mathrm{ch}} = 0.0$ (right).

Fig. 7: Dependence of curvatures on the strength of the surface elasticity. Snapshots of tissues at $t = 2.0$ are shown for cases with several values of the surface elasticity: $k^{\mathrm{ch}} = 2.56 \times 10^{-2}$ (a), 2.56×10^{-1} (b), 2.56×10^{0} (c) and 2.56×10 (d). Colors on the apical and basal surfaces indicate mean curvatures, C_{H}.

Fig. 8: Dependence of curvatures on the strength of the apical contractility. (a) Standard deviations (SDs) of mean curvatures, C_{H}, as a function of apical contractility, k^{ac}. SDs were measured on both apical surfaces (pink) and basal surfaces (blue). (b) The strains of cell apical widths as a function of k^{ac}. The strains were estimated from the square roots of the mean surface areas of apical polygons. (c–f) Cross-section of tissues at $t = 2.0$ in cases with varying $k^{\mathrm{ac}} = 10^{-3}$ (c), 10^{-2} (d), 10^{-1} (e), and 10^{0} (f). Colors on the apical and basal surfaces indicate C_{H}.

Table 1:

Symbol	Value	Description
Physical parameters for cell mechanical properties		
η	400	Friction coefficient of vertex (Eq.(1))
k^{cv}	20	Constant of cell volume elasticity (Eq.(8))
k^{cs}	2.56×10^{-2} – 2.56×10	Constant of cell surface elasticity (Eq.(10))
k^{ch}	0.0, 1.0	Constant of cell height elasticity (Eq.(12))
k^{ac}	0.0, 1.0×10^{-4}–10	Constant of apical circumferential length elasticity (Eq.(13))
v_0	5.0	Characteristic cell volume (Eq.(9))
γ_0^{cs}	1.3	Ratio of equilibrium cell surface area (Eq.(11))
$l_0^{\text{cell height}}$	5.0	Equilibrium cell height (Eq.(12))
γ_0^{ac}	0.5	Ratio of equilibrium circumferential length (Eq.(14))
$\tau_{\mathrm{ave}}^{\text{cell cycle}}$	1.0	Statistical average of cell cycle (Eq.(6))
ψ^{I}	0.6	Time ratio of state I (Eq.(9))
ψ^{II}	0.2	Time ratio of state II (Eq.(9))
ψ^{III}	0.1	Time ratio of state III (Eq.(9))
ψ^{IV}	0.1	Time ratio of state IV (Eq.(9))
Numerical parameters for computational simulations		
Δt	2.5×10^{-6}	Integration time step
Δt_{r}	5.0×10^{-6}	Time interval of network reconnections
Δl_{th}	0.05	Threshold length of network reconnections

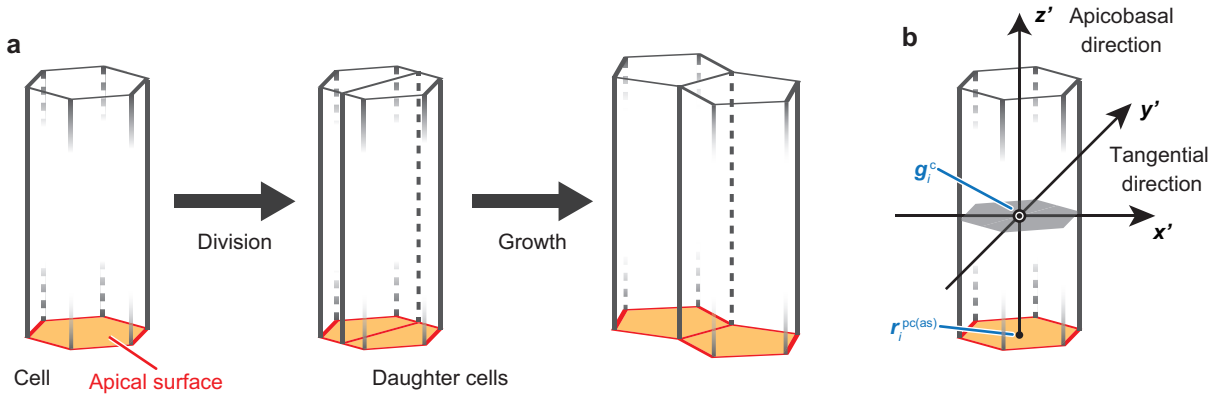

Volume elastic energy: $u_i^{\mathrm{cv}}\left(v_i^{\mathrm{c}}\right)=\frac{1}{2}k^{\mathrm{cv}}\left(\frac{v_i^{\mathrm{c}}}{v_{\mathrm{eq}\ i}^{\mathrm{c}}}-1\right)^2$

Surface elastic energy: $u_i^{\mathrm{cs}}\left(s_i^{\mathrm{c}}\right)=\frac{1}{2}k^{\mathrm{cs}}\left(\frac{s_i^{\mathrm{c}}}{s_{\mathrm{eq}\ i}^{\mathrm{c}}}-1\right)^2$

Height elastic energy: $u_i^{\mathrm{ch}}\left(l_i^{\mathrm{ch}}\right)=\frac{1}{2}k^{\mathrm{ch}}\left(\frac{l_i^{\mathrm{ch}}}{l_{\mathrm{eq}}^{\mathrm{ch}}}-1\right)^2$

Apical contractile energy: $u_i^{\mathrm{ac}}\left(l_i^{\mathrm{ac}}\right)=\frac{1}{2}k^{\mathrm{ac}}\left(\frac{l_i^{\mathrm{ac}}}{l_{\mathrm{eq}\ i}^{\mathrm{ac}}}-1\right)^2$

Figure 1:

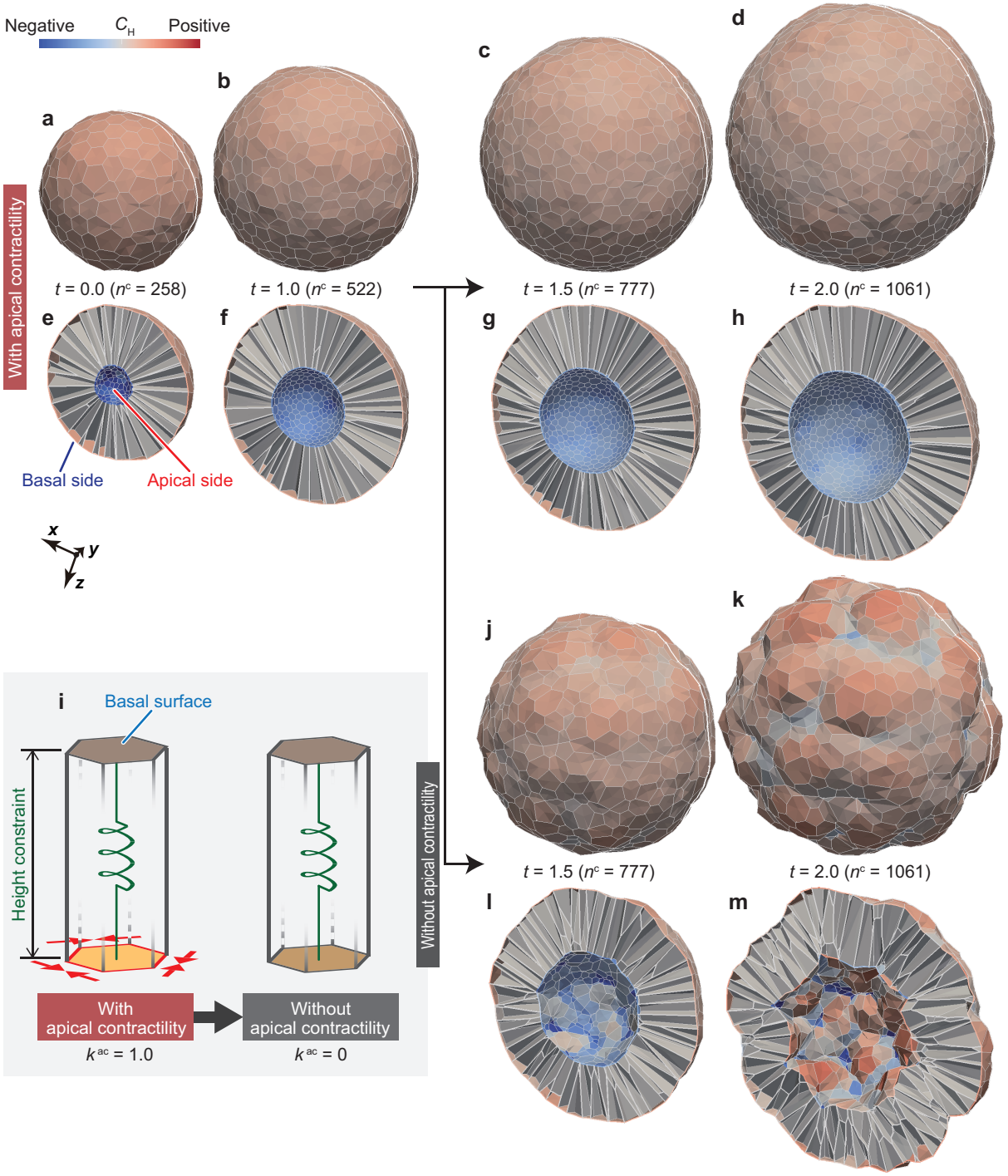
Negative
C_H
Positive
a
b
c
d
With apical contractility
t = 0.0 (n^c = 258)
t = 1.0 (n^c = 522)
t = 1.5 (n^c = 777)
t = 2.0 (n^c = 1061)
e
f
g
h
Basal side
Apical side
x
y
z
i
Basal surface
Height constraint
With apical contractility
k^{ac} = 1.0
Without apical contractility
k^{ac} = 0
Without apical contractility
j
k
t = 1.5 (n^c = 777)
t = 2.0 (n^c = 1061)
l
m

Figure 2:

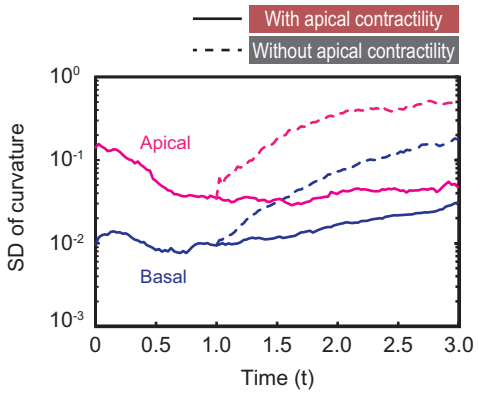

Figure 3:

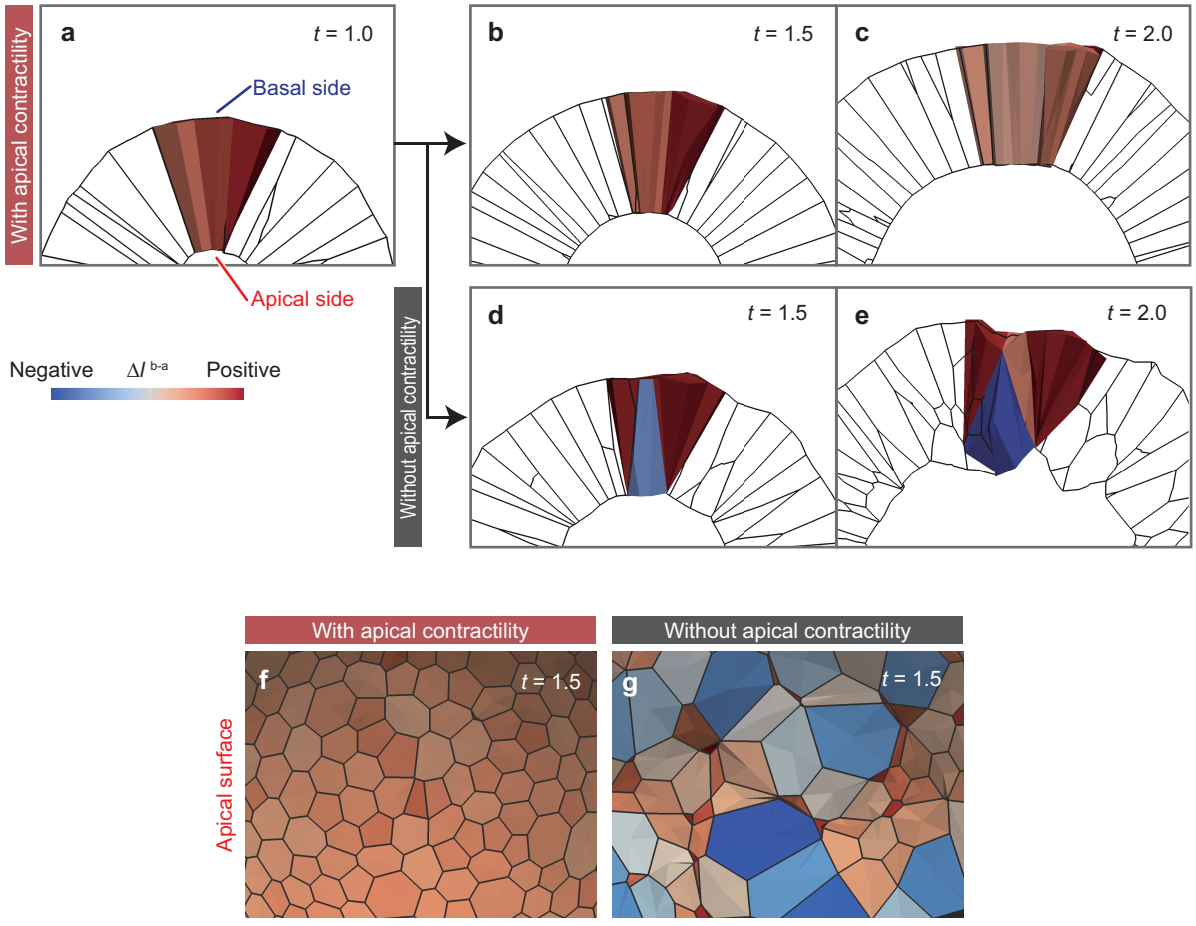

Figure 4:

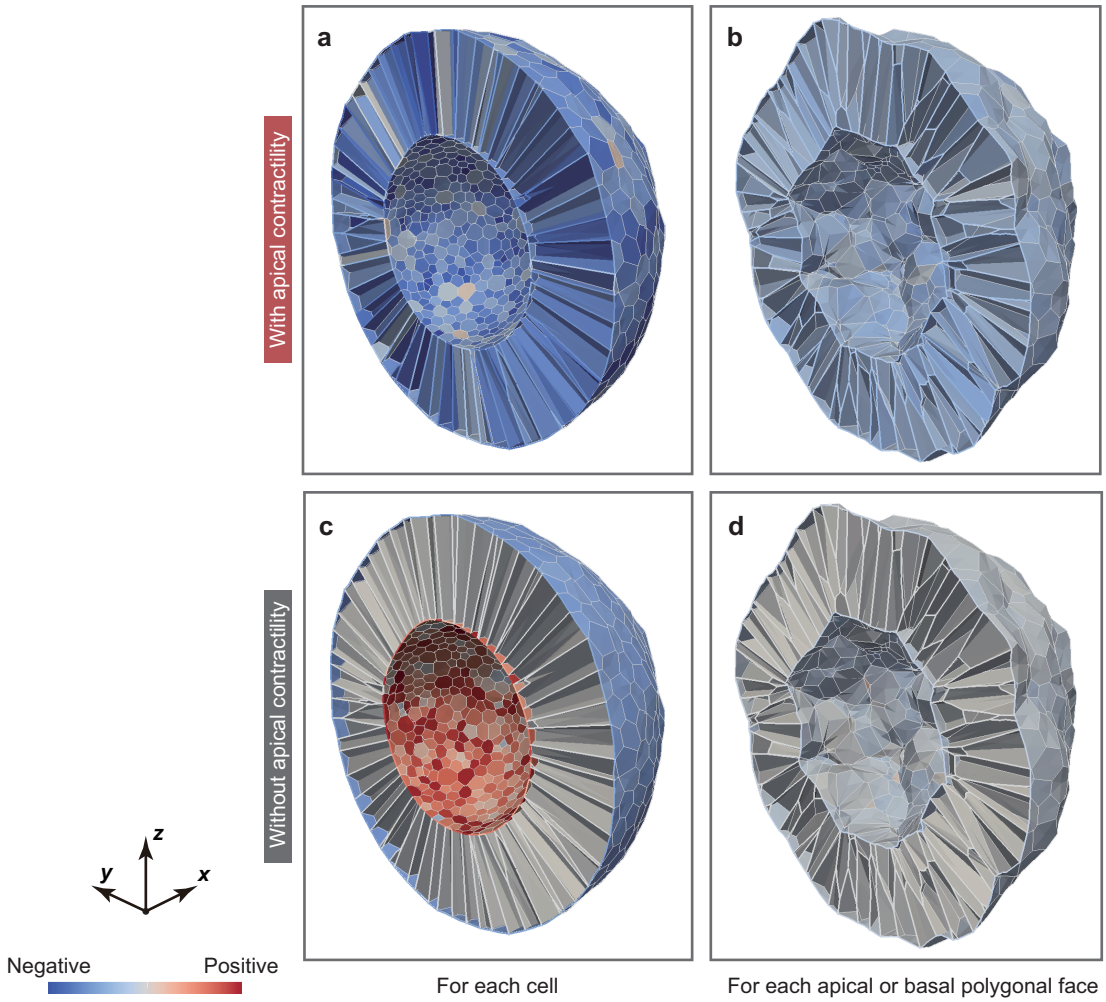
a
b
c
d
With apical contractility
Without apical contractility
z
y
x
Negative
Positive
For each cell
For each apical or basal polygonal face

Figure 5:

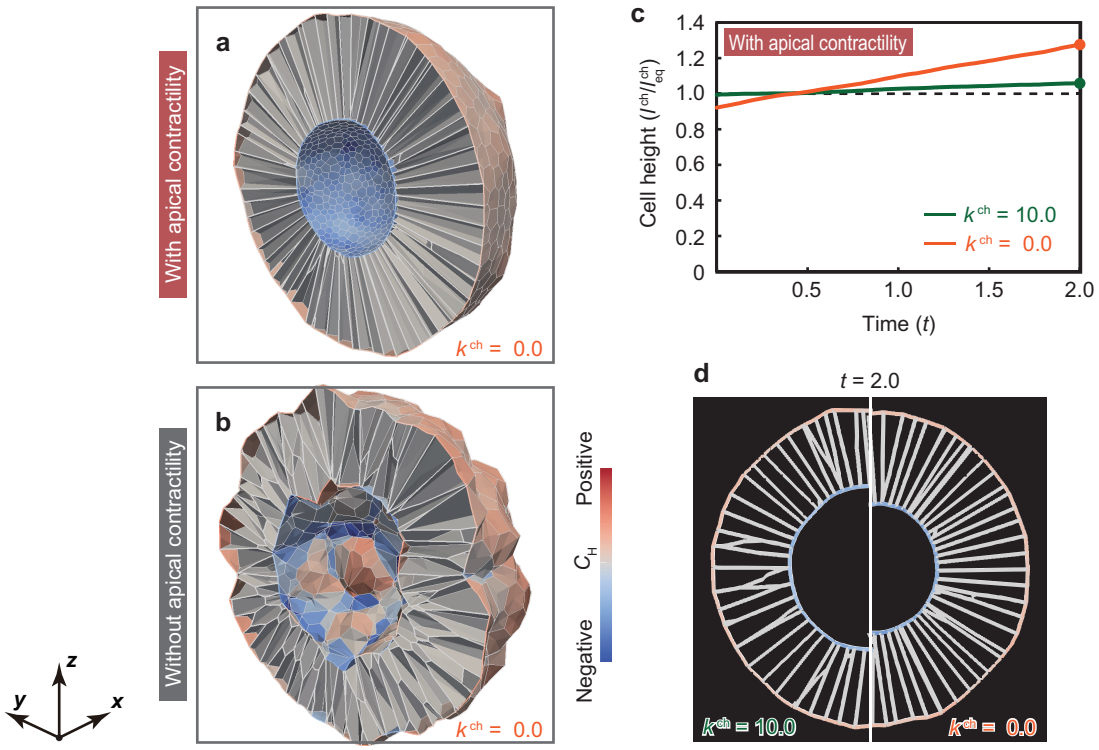

Figure 6:

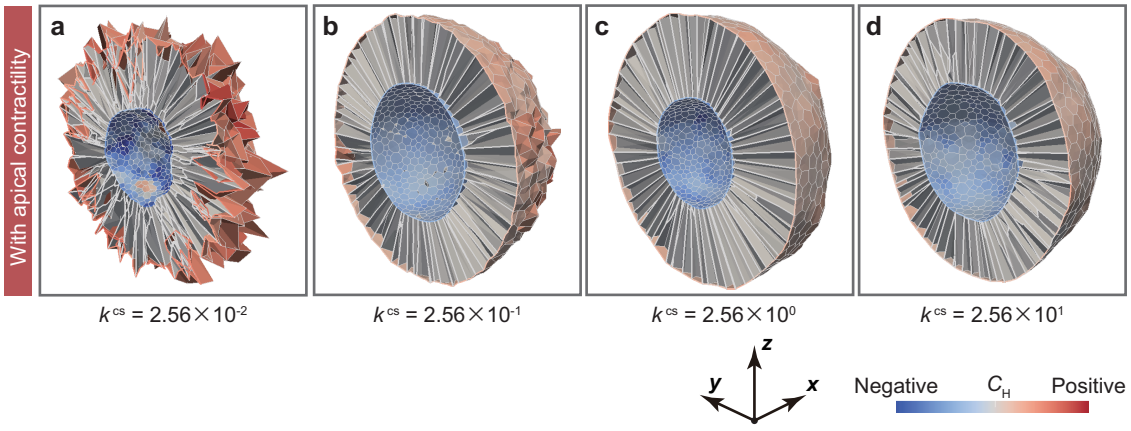

Figure 7:

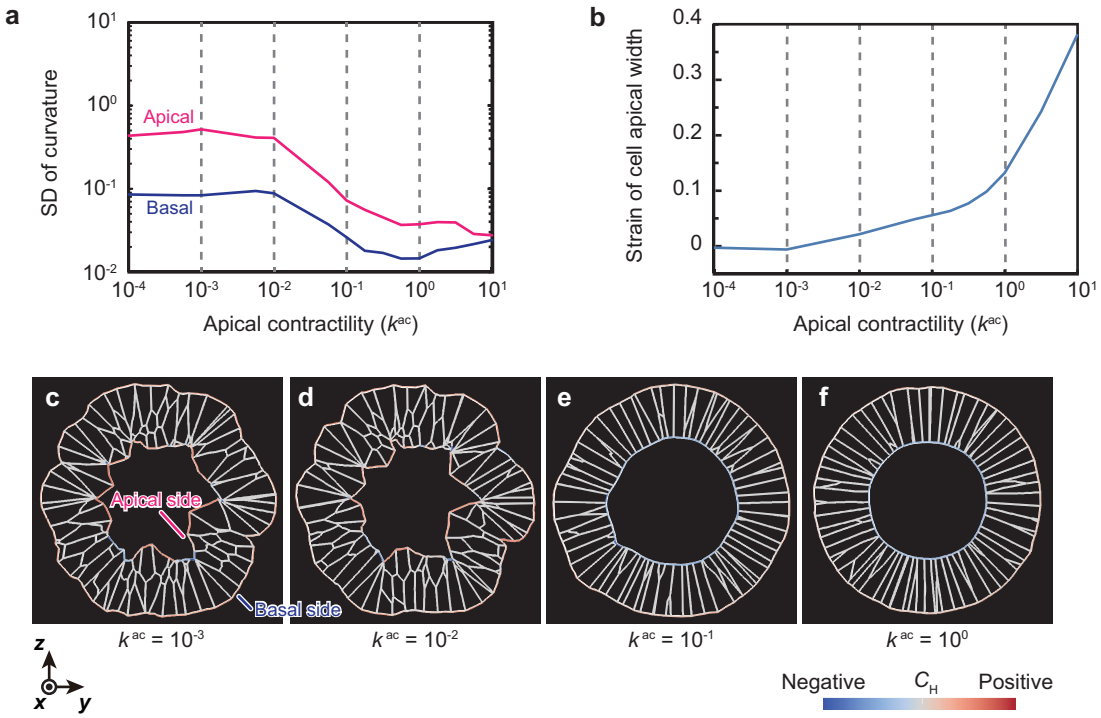
a
SD of curvature
Apical
Basal
Apical contractility (k^{ac})
b
Strain of cell apical width
Apical contractility (k^{ac})
c
d
e
f
Apical side
Basal side
$k^{ac} = 10^{-3}$
$k^{ac} = 10^{-2}$
$k^{ac} = 10^{-1}$
$k^{ac} = 10^{0}$
z
x
y
Negative
C_H
Positive

Figure 8:

Supplementary information

S1. Cell division manner

Cell division timing

To express cell divisions with spatiotemporally random timing, $\tau_i^{\text{cell div}}$ was determined to satisfy

$$\left\langle \tau_i^{\text{cell div}} \right\rangle = \tau_{\text{ave}}^{\text{cell cycle}}, \tag{6}$$

$$\left\langle (\tau_i^{\text{cell div}} - \tau_{\text{ave}}^{\text{cell cycle}})(\tau_j^{\text{cell div}} - \tau_{\text{ave}}^{\text{cell cycle}}) \right\rangle = \left(\tau_{\text{sd}}^{\text{cell cycle}}\right)^2 \delta_{ij}, \tag{7}$$

where $\langle ... \rangle$ indicates the statistical average and δ_{ij} is Kronecker's delta. The constants $\tau_{\text{ave}}^{\text{cell cycle}}$ and $\tau_{\text{sd}}^{\text{cell cycle}}$ represent the cell cycle time average and standard deviation, respectively. Such cell divisions will generate uncoordinated perturbations in the force balance among cells. In addition, to express cell growth, the cell cycle was separated into four states: I, II, III, and IV. The proportions of time spent in states I, II, III, and IV were represented by the constants ψ^{I}, ψ^{II}, ψ^{III}, and ψ^{IV} (≥ 0, $\psi^{\text{I}} + \psi^{\text{II}} + \psi^{\text{III}} + \psi^{\text{IV}} = 1$), respectively.

Intracellular position of a dividing plane

Assuming symmetric cell divisions, the intracellular position of a cell division was determined so that the dividing plane included the center of inertia of the ith cell, $\boldsymbol{g}_i^{\text{c}}$ (Fig. 1b).

Direction of a dividing plane

After cell division in the epithelium, daughter cells tend to locate in the direction of the longest axis of their mother cell shape within the plane of an epithelial sheet (Gibson et al., 2011). Thus, the normal vector of a cell-dividing plane is determined to be along the longest axis of the cell shape in the plane of the epithelial sheet. The longest axis is determined to be the eigenvector corresponding to the minimum eigenvalue of a cell inertia tensor estimated from the cell shape projected onto the plane normal to the apicobasal direction (Fig. 1b). The apicobasal direction, described by the z' axis, is defined as being along a vector from $\boldsymbol{g}_i^{\text{c}}$ to the polygonal center of an apical surface of individual cells, $\boldsymbol{r}_i^{\text{pc(as)}}$. This directional convention for the cell dividing plane has been described in the previous study (Okuda et al., 2012b).

S2. Cell potential energy

Cell volume elasticity

For cell volume elasticity, the current volume of the ith cell, v_i^{c}, was introduced. Then, the cell volume elastic energy, u_i^{cv}, was given by

$$u_i^{\text{cv}}\left(v_i^{\text{c}}\right) = \frac{1}{2} k^{\text{cv}} \left(\frac{v_i^{\text{c}}}{v_{\text{eq}\,i}^{\text{c}}} - 1 \right)^2, \tag{8}$$

which was similar to the expression used in other vertex model studies (Honda et al., 2004; Farhadifar et al., 2007; Honda et al., 2008a,b; Okuda et al., 2012a). The constant k^{cv} is volume elasticity. The variable $v_{\text{eq}\,i}^{\text{c}}$ is the equilibrium volume of the ith cell.

For the change in the equilibrium cell volume due to cell growth, the ith cell time t_i^{c} ($0 \leq t_i^{\text{c}} < \tau_i^{\text{cell div}}$) was defined as the time since the ith cell was generated by a cell division. The equilibrium cell volume of the ith cell, $v_{\text{eq}\,i}^{\text{c}}$, increased continuously according to t_i^{c}:

$$\frac{v_{\text{eq}\,i}^{\text{c}}\left(t_i^{\text{c}}\right)}{v_0^{\text{c}}} = \begin{cases} \dfrac{3}{4} + \dfrac{t_i^{\text{c}}}{4\psi^{\text{I}}\tau_i^{\text{cell div}}} & \text{I} \\ 1 & \text{II} \\ 1 + \dfrac{t_i^{\text{c}} - \left(\psi^{\text{I}} + \psi^{\text{II}}\right)\tau_i^{\text{cell div}}}{2\psi^{\text{III}}\tau_i^{\text{cell div}}} & \text{III} \\ \dfrac{3}{2} & \text{IV} \end{cases}. \tag{9}$$

Here the constant v_0^{c} is a characteristic cell volume.

Cell surface elasticity

For cell surface elasticity, the current surface of the ith cell, s_i^{c}, was introduced. Then, the cell surface elastic energy, u_i^{cs}, was given by

$$u_i^{\text{cs}}\left(s_i^{\text{c}}\right) = \frac{1}{2} k^{\text{cs}} \left(\frac{s_i^{\text{c}}}{s_{\text{eq}\,i}^{\text{c}}} - 1 \right)^2, \tag{10}$$

which was similar to the expression used in cell membrane modeling studies (Noguchi and Gompper, 2005; Ujihara et al., 2010). Here the constant k^{cs} is surface elasticity. The variable $s_{\text{eq}\,i}^{\text{c}}$ indicates an equilibrium surface area of the ith cell. Variable $s_{\text{eq}\,i}^{\text{c}}$ was defined by

$$s_{\text{eq}\,i}^{\text{c}} = \gamma^{\text{cs}} 4\pi \left(\frac{3 v_{\text{eq}\,i}^{\text{c}}}{4\pi} \right)^{\frac{2}{3}}, \tag{11}$$

where the constant γ^{cs} is a constant ratio of an equilibrium surface area to the surface area of an equivalent sphere with the same volume expressed by the variable $v_{\text{eq}\,i}^{\text{c}}$. When the constant γ^{cs} is close to one, the cell shape tends to be spherical because of the balance of forces between cell volume and surface elasticity in Eqs. (8) and (10).

Cell height elasticity

Epithelial thickness is often maintained during morphogenesis. When an epithelial sheet has a monolayer structure, the epithelial thickness corresponds to individual cells' heights. Therefore, we assumed that cell height was individually constrained by intracellular structures, such as the cytoskeleton. To express this cell height constraint, the current height of the ith cell, l_i^{ch}, was defined as the distance between the center points of the apical and basal surfaces (Fig. 1c). These center points of polygonal faces were defined in Eq. (3) in (Okuda et al., 2012a). Then, the cell height elastic energy, u_i^{ch}, was given by

$$u_i^{\text{ch}}\left(l_i^{\text{ch}}\right) = \frac{1}{2} k^{\text{ch}} \left(\frac{l_i^{\text{ch}}}{l_{\text{eq}}^{\text{ch}}} - 1 \right)^2. \tag{12}$$

Here the constant k^{ch} is cell height elasticity. The constant $l_{\text{eq}}^{\text{ch}}$ indicates the equilibrium cell height.

Apical contractility

To express apical contractility induced by circumferential actomyosin belt, the current circumferential length of the apical surface of the ith cell, l_i^{ac}, was introduced (Fig. 1c). Then, the apical contractile energy, u_i^{ac}, was given by

$$u_i^{\mathrm{ac}}\left(l_i^{\mathrm{ac}}\right) = \frac{1}{2}k^{\mathrm{ac}}\left(\frac{l_i^{\mathrm{ac}}}{l_{\mathrm{eq}\ i}^{\mathrm{ac}}} - 1\right)^2, \tag{13}$$

which was similar to the expression used in a two-dimensional vertex model study (Farhadifar et al., 2007). Here the constant k^{ac} is apical circumferential length elasticity.

The variable $l_{\mathrm{eq}\ i}^{\mathrm{ac}}$ is an equilibrium circumferential length of the ith cell. If the reference circumferential lengths of cell apical surfaces were constant, cells would sharpen to be cone-like shapes due to the increase in cell volume caused by cell growth. Such cell deformations during cell growth are not natural in typical epithelial cell behaviors. Thus, we assumed an approximately homothetic reference shape for cells during cell growth, and then variable $l_{\mathrm{eq}\ i}^{\mathrm{ac}}$ was defined as a function of $v_{\mathrm{eq}\ i}^{\mathrm{c}}$ by

$$l_{\mathrm{eq}\ i}^{\mathrm{ac}} = \gamma^{\mathrm{ac}} 2\pi \left(\frac{s_{\mathrm{eq}\ i}^{\mathrm{c\ equal}}}{\pi}\right)^{\frac{1}{2}}, \tag{14}$$

where constant γ^{ac} is a constant ratio of the equilibrium apical circumferential length to the circumferential length of an equivalent circle with the same surface area expressed by the variable $s_{\mathrm{eq}\ i}^{\mathrm{c\ equal}} (= v_{\mathrm{eq}\ i}^{\mathrm{c}} / l_{\mathrm{eq}}^{\mathrm{ch}})$.